Environmental Science & Technology

Article

pubs.acs.org/est

Reduction of Diffusive Contaminant Emissions from a Dissolved Source in a Lower Permeability Layer by Sodium Persulfate Treatment

Bridget A. Cavanagh,[†] Paul C. Johnson,*[,†] and Eric J. Daniels[‡]

[†]School of Sustainable Engineering and the Built Environment, Ira A Fulton Schools of Engineering, Arizona State University, Tempe, Arizona 85287, United States

[‡]Chevron Energy Technology Company, San Ramon, California 94583, United States

Downloaded via HOHAI UNIV on October 29, 2025 at 12:55:30 (UTC).
See https://pubs.acs.org/sharingguidelines for options on how to legitimately share published articles.

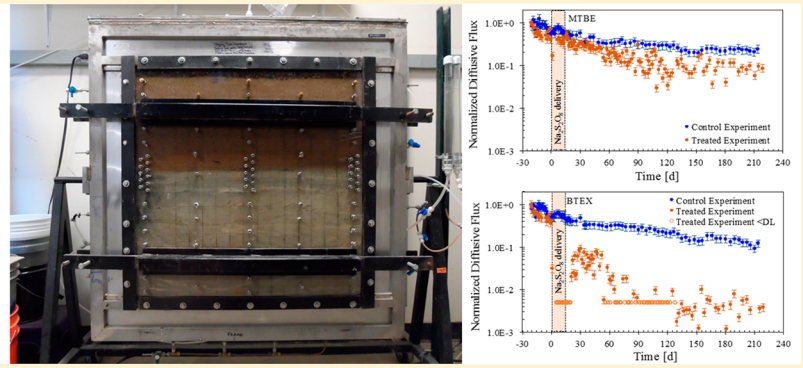

ABSTRACT: Residual contamination contained in lower permeability zones is difficult to remediate and can, through diffusive emissions to adjacent higher permeability zones, result in long-term impacts to groundwater. This work investigated the effectiveness of oxidant delivery for reducing diffusive emissions from lower permeability zones. The experiment was conducted in a 1.2 m tall × 1.2 m wide × 6 cm thick tank containing two soil layers having 3 orders of magnitude contrast in hydraulic conductivity. The lower permeability layer initially contained dissolved methyl *tert*-butyl ether (MTBE) and benzene, toluene, ethylbenzene, and *p*-xylenes (BTEX). The treatment involved delivery of 10% w/w nonactivated sodium persulfate ($Na_2S_2O_8$) solution to the high permeability layer for 14 days. The subsequent diffusion into the lower permeability layer and contaminant emission response were monitored for about 240 days. The $S_2O_8^{2-}$ diffused about 14 cm at 1% w/w into the lower permeability layer during the 14 day delivery and continued diffusing deeper into the layer as well as back toward the higher−lower permeability interface after delivery ceased. Over 209 days, the $S_2O_8^{2-}$ diffused 60 cm into the lower permeability layer, the BTEX mass and emission rate were reduced by 95−99%, and the MTBE emission rate was reduced by 63%. The overall treatment efficiency was about 60−110 g-$S_2O_8^{2-}$delivered/g-hydrocarbon oxidized, with a significant fraction of the oxidant delivered likely lost by back-diffusion and not involved in hydrocarbon destruction.

INTRODUCTION

According to USEPA,[1] the most frequently used in situ soil and groundwater remediation methods at Superfund sites between 2008 and 2011 include soil vapor extraction, pump and treat, and chemical treatment. These emphasize the treatment of more permeable subsurface zones at cleanup sites as they rely on fluid flow for removal of contaminants and/or delivery of reactants. If the lower permeability zones are not also fully remediated, groundwater may still be impacted for decades by diffusive emissions.[2−11]

Complete remediation of lower permeability layers is impracticable with the current technology at many sites. Alternative strategies involve: (a) partial source treatment into the lower permeability layer and (b) active treatment at the higher−lower permeability interface, both of which are intended to reduce emissions to the permeable zones to acceptable levels. For example, Marble et al.[12] report on TCE flux reduction from lower permeability soils after partial treatment by permanganate, and Clifton et al.[11] report on experiments in which the diffusive emission of benzene from a nonaqueous phase liquid-impacted lower permeability layer was reduced by about 90% by aerobic biodegradation while dissolved oxygen was being delivered by water flowing through the adjacent permeable layer.

This work focuses on partial source treatment of lower permeability layers containing dissolved and sorbed contaminants. Situations like this exist in dissolved plumes downgradient of NAPL source zones and in source zones where the NAPL has been largely removed by prior treatment or natural

Received: August 31, 2014
Revised: November 3, 2014
Accepted: November 11, 2014
Published: November 11, 2014

 © 2014 American Chemical Society dx.doi.org/10.1021/es5040443 | Environ. Sci. Technol. 2014, 48, 14582−14589

attenuation. The concept studied involves dissolved oxidant delivery to higher permeability zone(s), which leads to diffusive loading of oxidant in the lower permeability zones, eventual destruction of the contaminants, and reduced emissions.

In situ chemical oxidation (ISCO) use has increased since early applications in 1984.[13,14] The oxidant is typically dissolved in liquid solution and injected under pressure into wells but may also be delivered in gas phase. Its distribution is controlled by soil structure[14] and changes in soil properties resulting from chemical oxidation reactions, such as gas generation and precipitate formation. With increasing subsurface heterogeneity, remediation becomes more difficult.[15] ISCO delivery by diffusion into lower permeability layers has been discussed, with emphasis on permanganate to treat dense nonaqueous phase liquid sources.[7,12,16−19]

For petroleum hydrocarbon-impacted sites that are the focus of this work, the most relevant oxidants are hydrogen peroxide (H_2O_2), ozone (O_3), oxygen (O_2), and persulfate ($S_2O_8^{2-}$).[14] Permanganate is used for ISCO treatment but was not considered because it does not treat benzene.[14] Dissolved contaminants driving current groundwater remediation decisions are MTBE (methyl *tert*-butyl ether) and BTEX (benzene, toluene, ethylbenzene, xylenes). Of the oxidants, H_2O_2 and O_3 are unlikely to be of use for diffusive delivery given their fast and nonspecific reaction rates.[20]

Sodium persulfate has a desirable combination of high solubility and moderate reaction rate. Its aqueous solubility is about 11 000 times greater than O_2 (550 000 mg/L as $Na_2S_2O_8$ or about 440 000 mg/L $S_2O_8^{2-}$), and it is relatively more persistent and selective for petroleum hydrocarbon compounds than O_3 and H_2O_2.[21] Persulfate decomposition also leads to sulfate (SO_4^{2-}) production,[22] which can be an electron acceptor in petroleum hydrocarbon biodegradation reactions.

Persulfate can oxidize organics through "unactivated" electron transfer, although at a relatively slow rate.[14] The reaction rate of $S_2O_8^{2-}$ with dissolved hydrocarbons can be increased by "activation" strategies, which include elevating the temperature or adding chemicals such as highly alkaline fluid, ferrous iron, and hydrogen peroxide.[22]

The use of $S_2O_8^{2-}$ for diffusive delivery has been of recent interest. For example, Johnson et al.[22] modeled heat-activated $S_2O_8^{2-}$ diffusion into lower permeability layers and concluded that, at temperatures >50 °C, relatively short lifetimes of sulfate radicals limit diffusive delivery distances to a few cm. Tsitonaki et al.[18] suggested that nonactivated applications of $S_2O_8^{2-}$ may be preferable for remediation of lower permeability zones because a slower reaction rate favors increased oxidant penetration by diffusion. Merker[23] found that $S_2O_8^{2-}$ was able to diffuse 6 cm into Palouse loess in 85 d after interface treatment with 0.1 M $S_2O_8^{2-}$ solution. This work is complementary in that it focuses on treatment of lower permeability layers containing dissolved and sorbed contaminants and is unique in that effects of treatment on diffusive contaminant emissions are quantified.

EXPERIMENTAL DESIGN

Treatment and control experiments were conducted using the two-dimensional physical model shown schematically in Figure 1. The tank was prepared with two horizontal water-saturated layers: an upper higher-permeability layer and a lower lower-permeability layer source zone. The aquifer materials were selected to achieve about a 1000× permeability contrast so that lateral flow would occur through the higher permeability layer

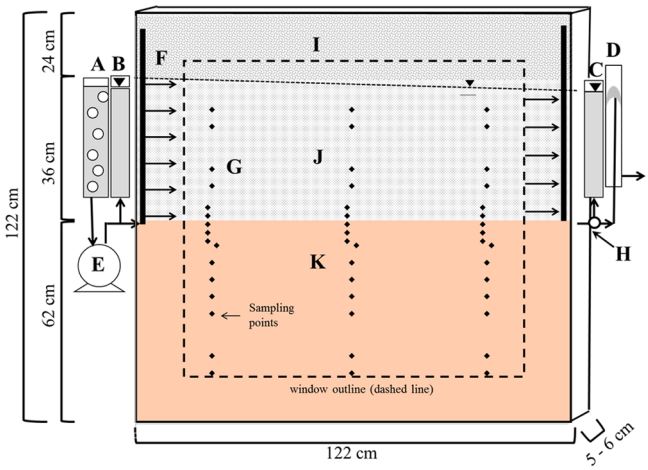

Figure 1. Experimental apparatus. (A) N_2 sparging system; (B) and (C) influent and effluent head measurement; (D) constant head device; (E) influent pump; (F) influent and effluent well screens; (G) sampling ports for water; (H) effluent sampling port; (I) pebbles to limit capillary rise; (J) higher permeability layer; (K) lower permeability layer.

with insignificant flow through the lower permeability layer. Influent, effluent, and in-tank dissolved concentrations of contaminants and oxidant, as well as flow rate and hydraulic head difference, are monitored with time. The diffusive emission flux [mg/cm^2-d] from the lower- to higher-permeability layer was determined by mass balance as in Clifton et al.[11] knowing the effluent flow rate and dissolved hydrocarbon concentration, where the emission flux = effluent flow rate [L/d] × effluent dissolved concentration [mg/L]/interface area [cm^2].

The use of nonactivated $S_2O_8^{2-}$ was evaluated on the basis of the work discussed above and wanting to maximize $S_2O_8^{2-}$ delivery throughout the lower permeability layer. Although no activator was added, it is possible that activation by ferrous iron occurred via release of ferrous iron from minerals in the soil.[14] Separate treated and untreated (control) experiments were conducted using the same tank and lower permeability layer to measure baseline emissions with no oxidant treatment and emissions after oxidant treatment.

Aquifer Physical Model Design. The stainless steel tank is 122 cm tall, 122 cm wide, and 5 cm thick for the first 15 cm in from the edges and 6.35 cm thick across the 92 cm wide window installed to view packing conditions and flow. Sampling ports through the window allow water collection for determining oxidant and chemical distribution. There is also a sampling port on the effluent line. Geoprobe stainless steel screen vapor/groundwater sampling implants (53 cm long × 1.3 cm diameter) were used as flow manifolds at the influent and effluent sides of the higher permeability layer. A constant 2.8 mL/min flow was controlled by a peristaltic pump at the inlet, and the saturated thickness was controlled by a constant head device at the outlet.

The higher-permeability layer was Quikrete Play Sand (99−99.9% by weight crystalline silica retained in 50 mesh sieve) with measured hydraulic conductivity $K = 6 \times 10^{-2}$ cm/s, porosity $\phi_T = 0.37$ cm^3-pores/cm^3-soil, and fraction of organic carbon $f_{oc} = 0.005$ g-carbon/g-soil. The lower-permeability bottom layer was 20% w/w 200 mesh silica sand mixed with 80% w/w 120 mesh feldspar sand with measured $K = 8 \times 10^{-5}$ cm/s, $\phi_T = 0.34$ cm^3-pores/cm^3-soil, and $f_{oc} = 0.004$ g-carbon/

dx.doi.org/10.1021/es5040443 | Environ. Sci. Technol. 2014, 48, 14582−14589

g-soil. The permeability contrast was about 3 orders of magnitude, and with the 0.16 cm head difference across the tank, the estimated average horizontal velocity through the lower permeability layer was <10 cm/y.

The dissolved-sorbed hydrocarbon source zone was created by flooding the tank from the bottom up with a dissolved solution of MTBE and BTEX at concentrations similar to those in the vicinity of leaking underground fuel tanks[24] until a steady and uniform concentration was measured in the lower permeability layer pore water. Then, lateral flow of N_2-sparged reverse-osmosis (RO) water was started in the higher-permeability layer.

A 10% w/w nonactivated $Na_2S_2O_8$ solution was pumped into the higher permeability layer for 14 d in the treated experiment. This concentration was selected as field applications reportedly use from 5% to 33.5% w/w $Na_2S_2O_8$ solutions.[25] The delivery time was selected after considering oxidant residence time in high permeability zones at field sites projected from representative treatment zone dimensions and groundwater flow rates (>15 d based on >10 m treatment zone length and <0.3 m/d groundwater velocities) and results from 1-D column experiments showing 10 cm of $S_2O_8^{2-}$ diffusion into a dissolved source in 14 d.[20] Modeling also suggested a limited benefit of longer delivery.[20]

Both control (no treatment) and treatment experiments were conducted using the same tank and lower permeability layer. The treatment experiment was conducted first. There was visual evidence that the oxidant solution delivery caused mobilization of fines in the higher permeability layer,[20] so it was replaced with fresh sand before starting the control experiment. Residual $S_2O_8^{2-}$ in the lower permeability layer was quenched with 30 g/L ascorbic acid between experiments[26] and before reintroducing MTBE and BTEX to the lower permeability layer. The ascorbic acid solution was gravity-fed from the bottom of the tank upward over 6 d until residual $S_2O_8^{2-}$ was not detected. Design parameters for treatment and control experiments are summarized in Table 1.

Tank Operations. During the treatment experiment, effluent water was sampled and analyzed daily for MTBE and BTEX until a pseudostable emission rate was established at about 26 d. Then, the background water flow was replaced with the 10% w/w $Na_2S_2O_8$ solution for 14 d. After that, clean N_2-sparged water was reintroduced for 203 d. Clean N_2-sparged water was introduced continuously for 239 d during the control experiment. A fluorescein dye tracer test was performed for both experiments to visually verify horizontal flow through the higher permeability layer and no flow through the lower permeability layer.

Table 1. Tank Operating Parameters

		control experiment	treatment experiment
higher permeability layer hydraulic conductivity K (cm/s)		6×10^{-2}	6×10^{-2}
lower permeability layer hydraulic conductivity K (cm/s)		8×10^{-5}	8×10^{-5}
average horizontal linear velocity in higher permeability layer observed with fluorescein tracer (m/d)		0.41	0.41
average horizontal linear velocity in lower permeability layer estimated from measured gradient, K, and porosity (m/d)		3×10^{-5}	3×10^{-5}
untreated period (d)		239	26
treatment duration (d)		0	14
post-treatment monitoring (d)		0	203
$Na_2S_2O_8$ concentration in aqueous solution (mg/L)		0	100 000
initial average dissolved concentrations in lower permeability layer (mg/L)	MTBE	37	41
	benzene	12	14
	toluene	20	26
	ethylbenzene	7	11
	p-xylene	7	8

Sample Collection and Analysis. Effluent sampling was performed either by collecting 3 mL from the effluent stream and diluting it into 27 mL of RO water or by collecting 30 mL from the effluent; larger volume samples were collected later to decrease detection levels. For the treatment experiment, the effluent was sampled daily for the first 155 d and thereafter every 4 d. After 155 d, 30 mL samples were collected and the sampling frequency was reduced. For the control tank, the change in sampling volume and frequency occurred after 55 d.

Water samples were also collected from the lower permeability layer before and after $S_2O_8^{2-}$ addition, 14 d after treatment, and each month. A needle connected to a 500 μL syringe was inserted through sampling ports into the pore space, and the plunger was pulled and held until the desired sample volume was collected (500 μL for hydrocarbon and 200 μL for $S_2O_8^{2-}$ analyses). Small sample volumes were used to minimize mass removal and downward advective flow induced by sampling; the cumulative volume removed by sampling was 1.1% and 1.6% of the total lower permeability pore space in the control and treated tanks, respectively. For hydrocarbon analyses, samples were diluted into 30 mL of RO water; if the sample contained $S_2O_8^{2-}$, 3 g of ascorbic acid was added to the vial prior to adding the hydrocarbon samples to quench possible hydrocarbon reactions with $S_2O_8^{2-}$.[26]

A gas chromatograph (GC) equipped with a flame ionization detector (FID) and a Restek MXT-5 30 m long × 0.53 mm ID column was used for heated headspace analyses (EPA method 8260B[27]) for MTBE and BTEX. The linear calibration range was between 0.005 and 10 mg/L. After considering dilution, it was 0.3 to 600 mg/L for 500 μL water samples, 0.05 to 100 mg/L for 3 mL effluent samples, and 0.005 to 10 mg/L for 30 mL samples. The analysis uncertainty for 3 and 30 mL effluent samples, as determined by duplicate and replicate analyses, was about ±21% with a 95% confidence level. The analysis uncertainty for 500 μL lower permeability layer samples was about ±30% at a 95% confidence level, with increased uncertainty reflecting difficulty in withdrawing water samples from the lower permeability layer due to slow flow and increased potential for aeration of the sample.

The $S_2O_8^{2-}$ concentration was quantified using the 0.01 N sodium thiosulfate iodometric titration method.[28] The analysis uncertainty was about ±7% based on duplicate sampling from the lower permeable region, with a detection level of about 0.04% w/w. The $S_2O_8^{2-}$ concentrations are reported below as $Na_2S_2O_8$ equivalents for direct comparison of in situ concentrations and injected solution concentrations.

RESULTS AND DISCUSSION

Effect of Treatment on Diffusive Emissions. Diffusive emission fluxes vs time for the $S_2O_8^{2-}$-treated and control tank experiments are shown in Figure 2. Individual BTEX component plots are available[20] but are presented here summed because they behaved similarly with time. Emission fluxes are normalized to their values at $t = -21$ d, which is after displacement of the dissolved contaminant feed solution from

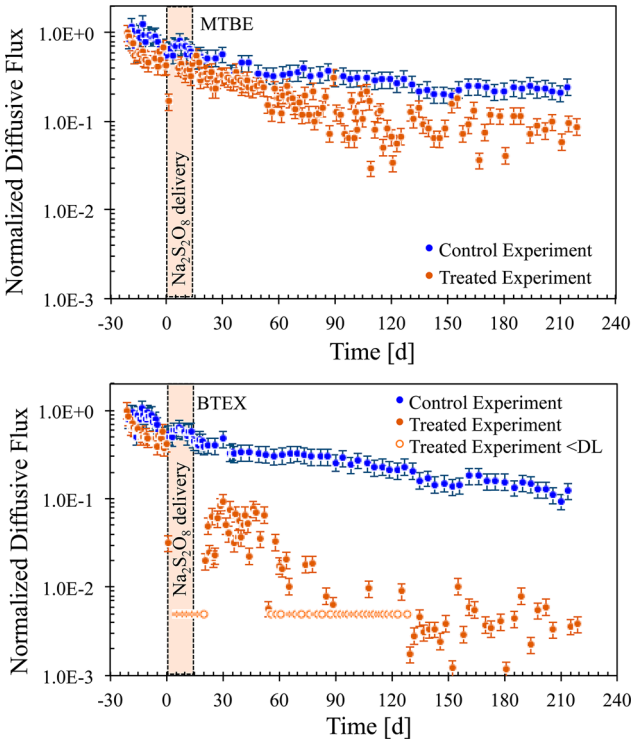

Figure 2. Comparison of normalized MTBE and BTEX emission rates from the $Na_2S_2O_8$-treated and control tanks. Detection limits ("DL") in the treated tank experiment decreased at t = 125 d with larger sample volumes.

the higher permeability layer by clean water. The $S_2O_8^{2-}$ delivery in the treated tank experiment occurs from t = 0 to t = 14 d. Error bars reflect ±21% uncertainty in effluent concentrations discussed above. Data points with unfilled centers indicate concentrations below the detection limit and are plotted at the detection limit. As mentioned above, the detection limit for the tank effluent concentration decreased when larger sampling volumes were collected. This occurred at t = 125 d and t = 25 d for the treated and control experiments, respectively.

The data in Figure 2 show that treatment resulted in reduced diffusive emissions relative to control conditions and that the emissions reduction was greater for BTEX than for MTBE. For example, 200 d after the end of $Na_2S_2O_8$ delivery, the normalized emission rate for MTBE in the treated tank was reduced by about 60% relative to the control, while the normalized diffusive emission rate for BTEX was reduced by 95−99% relative to the control. The difference in emissions reduction between MTBE and BTEX is consistent with previous findings suggesting that MTBE is less reactive than the BTEX compounds to persulfate oxidation reactions. For example, Liang et al.[30] studied persulfate treatment of MTBE and benzene in flow-through columns and observed less degradation of MTBE than benzene.

Concentration Profiles in the Lower Permeability Layers. To gain insight into the cause of diffusive emission reductions, MTBE, BTEX, and $S_2O_8^{2-}$ concentration profiles are presented in Figure 3 for a progression of sampling times. All concentrations are presented vs elevation (z) above the tank bottom, where z = 62 cm is the elevation of the high−low permeability interface. The concentrations presented are depth-specific averages across the left, center, and right vertical

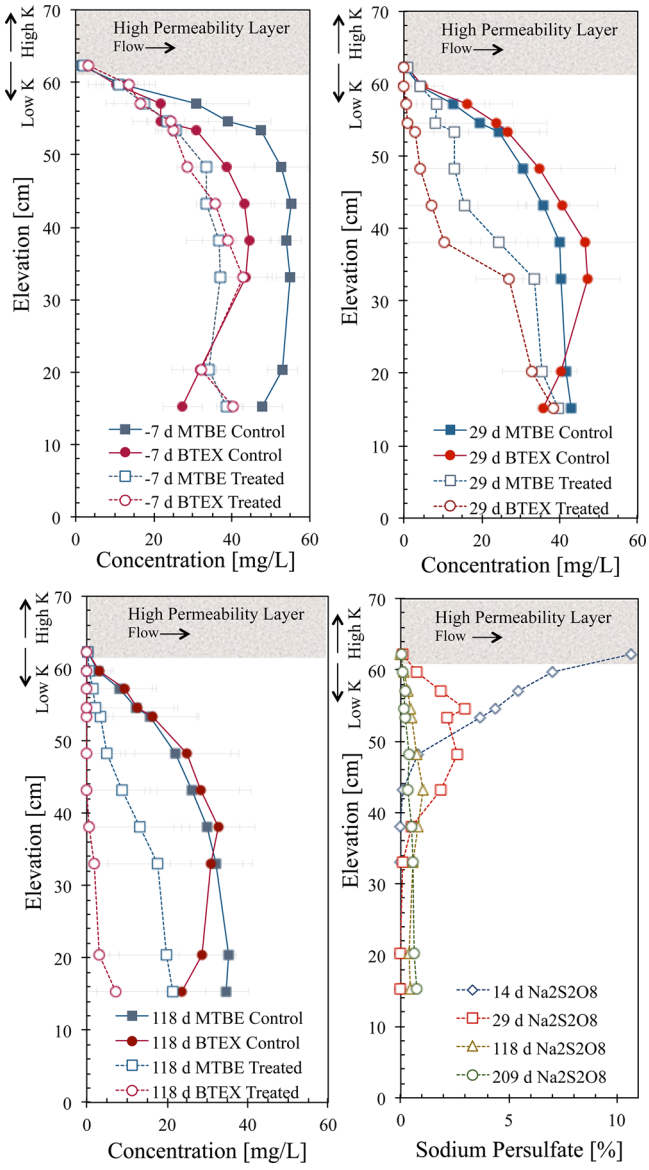

Figure 3. Depth-specific concentrations averaged across three vertical transects for MTBE, BTEX, and $S_2O_8^{2-}$ (presented as $Na_2S_2O_8$ equivalents) in the lower permeability layer. The high−low permeability interface is at the 62 cm elevation.

sampling transects shown in Figure 1. As with Figure 2, summed BTEX concentrations are presented because all components responded similarly and individual component data are available elsewhere.[20]

MTBE and BTEX profiles are presented for 1 week before $Na_2S_2O_8$ delivery (t = −7 d) and approximately 2 weeks (t = 29 d) and 104 d (t = 118 d) after ending $Na_2S_2O_8$ delivery. Concentration profiles are relatively similar for MTBE and BTEX in both treated and control experiments at t = −7 d, which is 7 d prior to oxidant delivery and 14 d after creating the source zone and initiating water flow across the higher permeability layer. The concentration gradient toward the high−low permeability interface evident in the upper 20 cm of the lower permeability layer in both experiments is expected with diffusive emissions to water flowing through the higher permeability layer. Approximately 2 weeks after $Na_2S_2O_8$ delivery (t = 29 d), the shape and magnitude of concentration profiles in the treated experiment differ significantly from those

dx.doi.org/10.1021/es5040443 | Environ. Sci. Technol. 2014, 48, 14582−14589

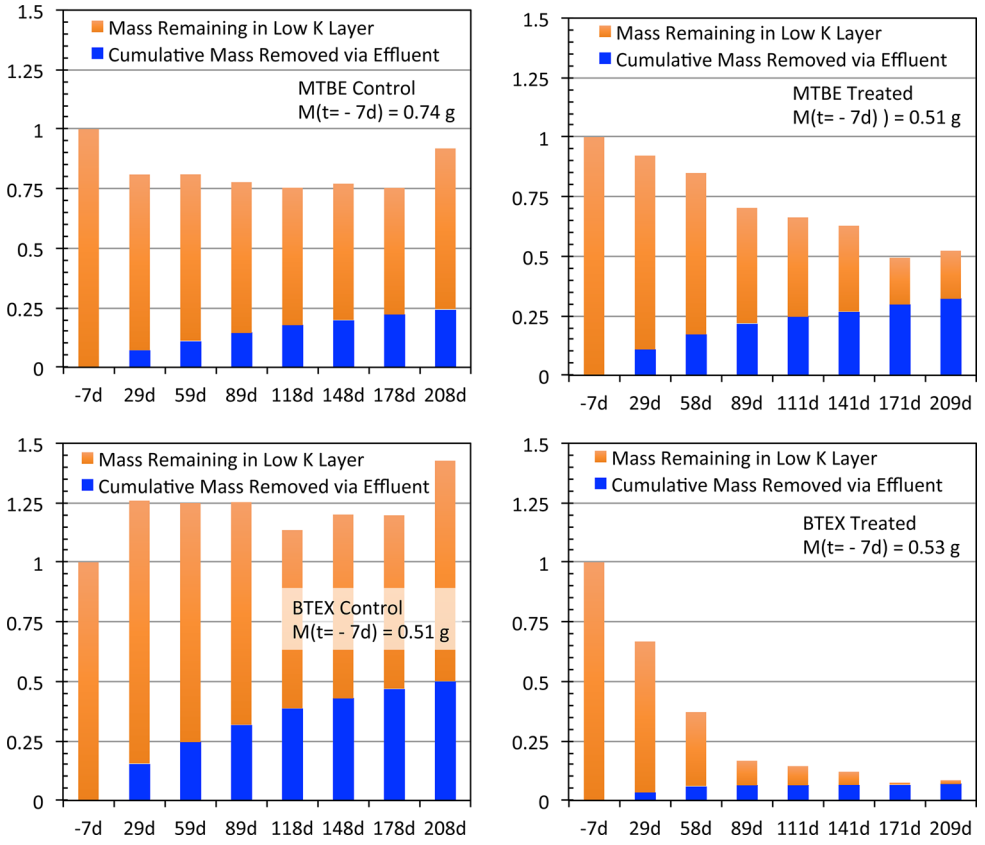

Figure 4. Mass balance results for control (left plots) and treatment (right plots) experiments, with results normalized to the dissolved source mass at $t = -7$ d.

in the control, and the differences grow with time. Concentration profiles in the control experiment change little from t = 29 d to t = 118 d, while BTEX and MTBE concentrations decline with time at all depths in the treatment experiment. Thus, concentration profiles suggest BTEX and MTBE destruction in the upper 20 cm of the lower permeability layer over a multiweek time frame. This concentration reduction near the interface then leads to lower concentration gradients and lower diffusive emissions. In the longer term, the 95−99% reduction in BTEX emissions appears to result from near-complete treatment of BTEX in the lower permeability layer. The differences in BTEX and MTBE emission reductions in Figure 2 are consistent with differences in treatment within the lower permeability layer shown in Figure 3.

The $S_2O_8^{2-}$ concentration profiles in the treated experiment are shown for four times, including: the end of $Na_2S_2O_8$ delivery (t = 14 d), approximately 2 weeks after ending delivery (t = 29 d), and then 104 and 195 d after ending delivery (t = 118 and 209 d). The t = 14 d profile shape appears as expected for transient diffusion-dominated delivery,[31] and $S_2O_8^{2-}$ was detected as far as 14 cm from the high−low permeability interface at >1% w/w concentrations. This is more rapid diffusion than that reported by Merker,[23] who observed about half the distance (6 cm) over a longer time (85 d) into Palouse loess with 0.1 M $S_2O_8^{2-}$ solution (about 25% of the 81 g-$S_2O_8^{2-}$/L used in this study). This could be due to the higher concentration gradient or lower natural organic demand present in this experiment. Concentration profiles suggested the possibility of density-driven migration in the top 6 cm of the center and right transect.

At t = 29 d, which follows 15 d of clean water flow through the higher permeability layer, the more bell-like shape of the concentration profile indicates $S_2O_8^{2-}$ diffusing in two directions: toward the high−low permeability interface and deeper into the lower permeability layer. The t = 29 d profile also corresponds roughly to the peak of the BTEX emissions rebound in Figure 2. By t = 118 d, $S_2O_8^{2-}$ was detected in the lowest sampling port 44 cm below the interface. After t = 118 d, $S_2O_8^{2-}$ persisted for three months at concentrations ranging from 0.1% to 1% w/w and was still present when the experiment was terminated. This is expected since reported half-lives of activated and nonactivated $S_2O_8^{2-}$ range from 0.15 to 700 d.[14]

Mass Balance Calculations. The dissolved mass of each hydrocarbon in the lower permeability layer was calculated by integrating concentration data with depth for the left, center, and right transects, multiplying the results by the porosity and relevant portion of the lower permeability interface area, and then summing these. The cumulative mass emitted from the lower permeability layer was calculated by integrating the diffusive emissions with time. For reference, uncertainties estimated for mass balance components are ±28% for the mass in the lower permeability layer and ±17% for the effluent loss mass calculations.

Figure 4 presents MTBE and BTEX results, normalized to dissolved masses in the lower permeability layer at $t = -7$ d. For chemicals with low sorption potential like MTBE, the initial dissolved mass is approximately equal to the total initial mass in the lower permeability zone. Consequently, the sum of the two normalized mass components should be unity for a control experiment and ≤1 for an experiment in which there is

dx.doi.org/10.1021/es5040443 | Environ. Sci. Technol. 2014, 48, 14582−14589

compound transformation. This is what is observed in Figure 4 for MTBE, where the sum of mass components is within experimental error of unity for the duration of the experiment and there is about 50% mass loss for the treatment experiment.

For chemicals with moderate sorption potential like BTEX components, the total mass in the lower permeability layer (M_T) is greater than the dissolved mass (M_D). When linear sorption partitioning is assumed, the two are related by $M_T = M_D \times (1 + K_s\rho_b/\phi_m)$, where K_s is a chemical- and soil-specific sorption coefficient [L-H_2O/kg-soil], ρ_b is the soil bulk density [kg-H_2O/L-soil], and ϕ_m is the water-saturated porosity [L-pores/L-soil]. Thus, in a control experiment where mass initially in the lower permeability layer is emitted (M_E), the sum of the normalized mass components increases with time according to $(M_D/M_D^o) + (M_E/M_D^o) = (M_D/M_D^o) + (1 - (M_D/M_D^o)) \times (1 + K_s\rho_b/\phi_m)$ and ultimately reaches $(1 + K_s\rho_b/\phi_m)$. While arguably not significant relative to error in mass calculations, results in Figure 4 suggest behavior like this for BTEX components in the control experiment, with $(K_s\rho_b/\phi_m)$ in the range of about 1 to 3. The significant difference between Figure 4 control and treated experiment plots for BTEX again indicate destruction as a result of treatment. The treatment experiment shows near-complete treatment of the lower permeability layer and >90% of the initial dissolved BTEX mass transformed by oxidation.

Intermediate and final breakdown products were not investigated in this work. Huang et al. report intermediates that include *tert*-butyl formate, *tert*-butyl alcohol, methyl acetate, and acetone from $S_2O_8^{2-}$ degradation of MTBE[29] and acetone from other hydrocarbons.[21]

Partitioning experiments were conducted to determine sorption coefficients for MTBE and the BTEX components in the lower permeability material. Those led to the conclusion that the K_s values were at least an order of magnitude lower than expected from typical correlations and likely <0.01 L-H_2O/kg-soil for MTBE and <0.2 L-H_2O/kg-soil for the BTEX components. Those results are consistent with Figure 4 plots. For example, for K_s = 0.2 L-H_2O/kg-soil, $(K_s\rho_b/\phi_m) = 1$ (ρ_b = 1.7 g/cm^3, ϕ_m = 0.34 cm^3-pores/cm^3-soil), which is consistent with the discussion above.

The $S_2O_8^{2-}$ concentration data were also integrated with depth to calculate the mass of $S_2O_8^{2-}$ in the lower permeability layer (M_P) with time. The results are presented in Figure 5, where the mass is normalized to the mass present when oxidant delivery ceased at t = 14 d (178 g). The $S_2O_8^{2-}$ mass declines by about 50% from t = 14 d to about t = 60 d and then more slowly after that. For reference, if $S_2O_8^{2-}$ were to be distributed uniformly throughout the lower permeability layer at its detection level of 0.04% w/w, then that would be equivalent to M_P/M_P (t = 14 d) = 0.38, which is close to the asymptote at the end of the experiment. The $S_2O_8^{2-}$ lost by back-diffusion to the higher permeability layer was not quantified as concentrations in effluent samples were below the detection limit.

In aggregate, 144 g of $S_2O_8^{2-}$ was present in the lower permeability layer after the 14 d delivery, 45% remained at t = 218 d, and 0.93 g (no sorption) to 1.5 g (estimating sorption with $(K_s\rho_b/\phi_m) = 1$ for BTEX) of hydrocarbon mass was lost from the lower permeability layer through back-diffusion and reaction. The hydrocarbon mass lost by back-diffusion was estimated from the effluent removal rate data from the treatment experiment (0.2 g). An overall treatment efficiency can be defined for the experiment as the (mass of $S_2O_8^{2-}$ delivered − mass of $S_2O_8^{2-}$ in the lower permeability layer at the end of the experiment)/mass of hydrocarbon degraded. Using the results above leads to values ranging from about 60 to 110 g-$S_2O_8^{2-}$/g-hydrocarbon. This is two to three times the theoretical efficiency of $S_2O_8^{2-}$ to benzene under well-mixed conditions (37 g-$S_2O_8^{2-}$/g-benzene) but is similar to batch reactor results published in Sra et al.[32] who report 120 (unactivated) and 130−340 (activated) g-$S_2O_8^{2-}$/g-hydrocarbon. Higher than theoretical values are to be expected here because of unquantified persulfate loss to back-diffusion and reactions with soil.

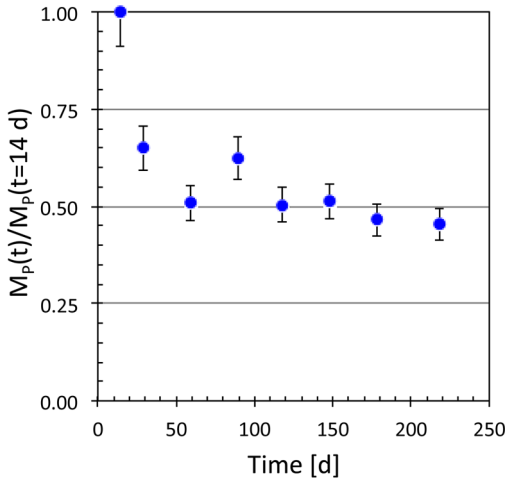

Figure 5. Normalized persulfate mass in the lower permeability layer at t = 14 d.

Given that the $S_2O_8^{2-}$ concentration profiles resemble behavior expected for diffusion with no reaction, a diffusion-only analytical model was used to explore how much of the $S_2O_8^{2-}$ disappearance might be the result of back-diffusion. For the case of diffusive transport into a semi-infinite medium, where the boundary experiences step changes in concentration at t = 0 and the end of loading time t_L, the concentration profile solution is of the form:[31,33]

$$C(z,t)/C^o = 0, \quad t < 0$$
$$= F(z,t), \quad 0 < t < t_L$$
$$= F(z,t) - F(z, t - t_L), \quad t \geq t_L$$

where C^o is the concentration at the high−low permeability interface between $0 < t < t_L$ and

$$F(z,t) = 1 - \mathrm{erf}(z/(\alpha t))^{0.5}$$

and erf(x) denotes the error function of x. Here, z is the distance from the interface and α depends on the effective diffusion coefficient, porosity, and partitioning and is used here as a fitting parameter. For Figure 6 results, α was adjusted to have the predicted $S_2O_8^{2-}$ concentration profile and mass at t = 14 d match experimental data, and then, that value was used for future predictions. The results suggest that the majority of the $S_2O_8^{2-}$ disappearance was the result of back-diffusion rather than reaction.

This study demonstrates that lower permeability layers impacted by dissolved BTEX and MTBE sources can be treated by diffuse loading of slowly reacting oxidants like sodium persulfate. Future work is needed to determine relationships between design parameters (e.g., oxidant concentration, loading time, layer thickness, dissolved concentrations) and emissions

dx.doi.org/10.1021/es5040443 | *Environ. Sci. Technol.* 2014, 48, 14582−14589

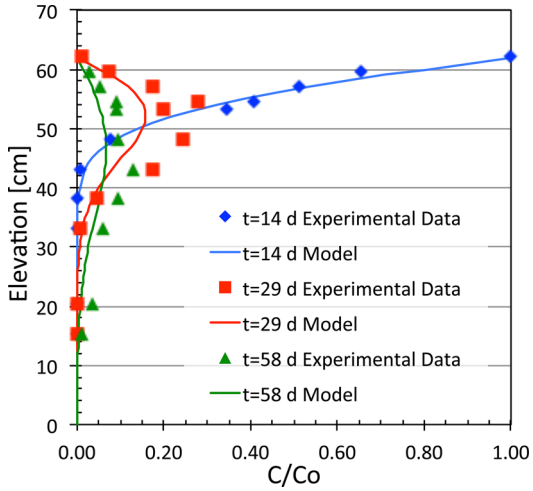

Figure 6. Predicted $Na_2S_2O_8$ concentration profiles based on a model fit of mass at t = 14 d.

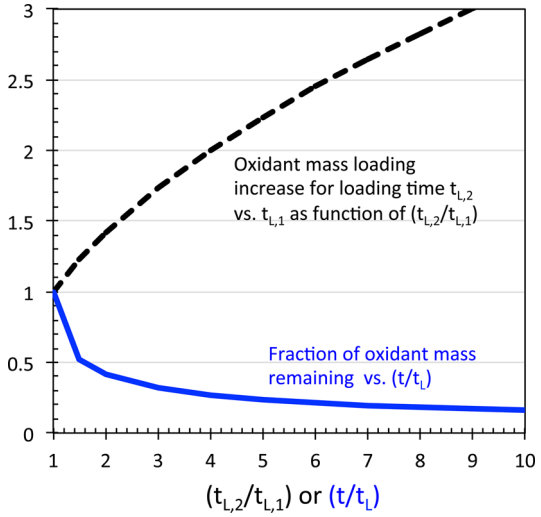

Figure 7. Increasing mass loading with time and increasing mass reduction with time.

reduction so that the process can be optimized, for example, with a minimization of oxidant used.

Along these lines, the analytical solution discussed above can be integrated with depth to estimate oxidant mass loading with time (t) as a function of loading time (t_L):

$$M(t) = 2\phi_m C^\circ \sqrt{\frac{D^{eff}}{\pi}}(\sqrt{t}) = 0; \quad t < t_L$$

$$M(t) = 2\phi_m C^\circ \sqrt{\frac{D^{eff}}{\pi}}(\sqrt{t} - \sqrt{t - t_L}); \quad t \geq t_L$$

where D^{eff} [cm^2/s] is the effective diffusion coefficient [cm^2/s] and C^o [g/cm^3] is the oxidant concentration at the interface. The effect of increasing the loading time on total mass delivered can be examined through:

$$\frac{M(t_{L,2})}{M(t_{L,1})} = \sqrt{\frac{t_{L,2}}{t_{L,1}}}$$

which suggests that 4× the loading time would be required to increase oxidant mass by 2×, independent of layer properties.

In addition, the fraction of oxidant mass remaining after loading has ceased is also independent of layer properties:

$$\frac{M(t)}{M(t_L)} = \sqrt{\frac{t}{t_L}} - \sqrt{\frac{t - t_L}{t_L}}$$

Master plots for these functions are presented in Figure 7.

AUTHOR INFORMATION

Notes

The authors declare no competing financial interest.

ACKNOWLEDGMENTS

This research was funded by Chevron Energy Technology Company.

REFERENCES

(1) United States Environmental Protection Agency. *Superfund remedy report*, fourteenth ed. (Soil Waste Emergency Response No. EPA 542-13-016); United States Environmental Protection Agency: Washington, DC, 2013.

(2) Mutch, R.; Scott, J.; Wilson, D. Cleanup of fractured rock aquifers: Implications of matrix diffusion. *Environ. Monit. Assess.* **1993**, *24*, 45−70.

(3) Parker, B.; McWhorter, D.; Cherry, J. Diffusive loss of non-aqueous phase organic solvents for idealized fracture networks in geologic media. *Ground Water* **1997**, *35* (6), 1077−1088.

(4) Liu, C.; Ball, W. Back diffusion of chlorinated solvent contaminants from a natural aquitard to a remediated aquifer under well-controlled field conditions: Predictions and measurements. *Ground Water* **2002**, *40* (2), 175−184.

(5) Chapman, S.; Parker, B. Plume persistence due to aquitard back diffusion following dense nonaqueous phase liquid source removal or isolation. *Water Resour. Res.* **2005**, *41*, 1−16.

(6) Lipson, D.; Kueper, B.; Gefell, M. Matrix diffusion-derived plume attenuation in fractured bedrock. *Ground Water* **2005**, *43* (1), 30−39.

(7) Honning, J.; Broholm, M.; Bjerg, P. Role of diffusion in chemical oxidation of pce in a dual permeability system. *Environ. Sci. Technol.* **2007**, *41* (24), 8426−8432.

(8) Parker, B.; Chapman, S.; Guibeault, M. Plume persistence caused by back diffusion from thin clay layers in a sand aquifer following tce source-zone hydraulic isolation. *J. Contam. Hydrol.* **2008**, *102* (1−2), 86−104.

(9) Singh, R.; Olson, M. S. Transverse chemotactic migration of bacteria from high to low permeability regions in a dual permeability microfluidic device. *Environ. Sci. Technol.* **2012**, *46*, 188−3195.

(10) Schaefer, C.; Towne, R.; Lippincott, D.; Lazouskaya, V.; Fischer, T.; Bishop, M.; Dong, H. Coupled diffusion and abiotic reaction of trichloroethene in minimally disturbed rock matrices. *Environ. Sci. Technol.* **2013**, *47*, 4291−4298.

(11) Clifton, L.; Dahlen, P.; Johnson, P. C. Effect of dissolved oxygen manipulation on diffusive emissions from NAPL-impacted lower permeability soil layers. *Environ. Sci. Technol.* **2014**, *48* (9), 1−27.

(12) Marble, J.; Carroll, K.; Janousek, H.; Brusseau, M. In situ oxidation and associated mass-flux-reduction/mass removal behavior for systems with organic liquid located in lower-permeability sediments. *J. Contam. Hydrol.* **2010**, *117*, 82−93.

(13) Krembs, F.; Siegrist, R.; Crimi, M.; Furrer, R.; Petri, B. ISCO for groundwater remediation: Analysis of field applications and performance. *Ground Water Monit. Rem.* **2010**, *30* (4), 42.

(14) Siegrist, R.; Crimi, M.; Brown, R. *In situ chemical oxidation for groundwater remediation*; Springer Science Business Media LLC: New York, 2011.

(15) National Research Council of the National Academes, Ed. *Alternatives for managing the nation's complex contaminated groundwater sites*; The National Academies Press: Washington DC, 2013.

(16) Siegrist, R.; Lowe, K.; Murdoch, L.; Case, T.; Pickering, D. In situ oxidation by fracture emplaced reactive solids. *J. Environ. Eng.* **1999**, *125* (5), 429−440.
(17) Struse, A.; Siegrist, R.; Dawson, H.; Urynowicz, M. Diffusive transport of permanganate during in situ oxidation. *J. Environ. Eng.* **2002**, *128* (4), 327−334.
(18) Tsitonaki, A.; Petri, B.; Crimi, M.; Mosbaek, H.; Siegrist, R.; Bjerg, P. In situ chemical oxidation of contaminated soil and groundwater using persulfate: A review. *Environ. Sci. Technol.* **2010**, *40* (1), 55−91.
(19) Chokerjaroenrat, C.; Kananizadeh, N.; Sakulthaew, C.; Comfort, S.; Li, Y. . Improving the sweeping efficiency of permanganate in lower permeable zones to treat TCE: Experimental results and model development. *Environ. Sci. Technol.* **2013**, *47* (22), 13031−13038.
(20) Cavanagh, B. C. Use of interface treatment to reduce emissions from residuals in lower permeability zones to groundwater flowing through more permeable zones. Ph.D. dissertation, Arizona State University, Tempe, Arizona, 2014.
(21) Huang, K.; Zhao, Z.; Hoag, G.; Dahmani, A.; Block, P. Degradation of volatile organic compounds with thermally activated persulfate oxidation. *Chemosphere* **2005**, *61* (4), 551−560.
(22) Johnson, R.; Tratnyek, P.; Johnson, R. Persulfate persistence under thermal activation conditions. *Environ. Sci. Technol.* **2008**, *42* (24), 9350−9356.
(23) Merker, M. Persulfate transport in two low-permeability soils. Master's thesis, Washington State University, Pullman, Washington, 2010.
(24) Johnson, P. C.; Kemblowski, M.; Colthart, J. Quantitative analysis for the cleanup of hydrocarbon-contaminated soils by in-situ venting. *Ground Water* **1990**, *28* (3), 413−429.
(25) Krembs, F. Critical analysis of the field-scale application of in situ chemical oxidation for the remediation of contaminated groundwater. Master's Thesis, Colorado School of Mines, Golden, Colorado, 2008.
(26) Huling, S.; Ko, S.; Pivetz, B. Groundwater sampling at ISCO sites: Binary mixtures of volatile organic compounds and persulfate. *Ground Water Monit. Rem.* **2011**, *31* (2), 72−79.
(27) United States Environmental Protection Agency. *Method 8260B: Volatile organic compounds by gas chromotography/mass spectrometry (GC/MS)*; United States Environmental Protection Agency: Washington, DC, 1996 .
(28) Wahba, N.; El Asnar, M. F.; El Sadr, M. M. Iodometric method for determination of persulfates. *Anal. Chem.* **1959**, *31* (11), 1870−1871.
(29) Huang, K.; Couttenye, R.; Hoag, G. Kinetics of heat-assisted persulfate oxidation of methyl tert-butyl ether (MTBE). *Chemosphere* **2002**, *49*, 413−420.
(30) Liang, S.; Kao, C.; Kuo, Y.; Chen, K.; Yang, B. In situ oxidation of petroleum-hydrocarbon contaminated groundwater using passive ISCO system. *Water Res.* **2011**, *45*, 2496−2506.
(31) Parker, B.; Gillham, R.; Cherry, J. Diffusive disappearance in immiscible-phase organic liquid in fractured geologic media. *Ground Water* **1994**, *32* (5), 805−820.
(32) Sra, K.; Thomson, N.; Varker, J. Persulfate treatment of dissolved gasoline compounds. *J. Hazard., Toxic, Radioact. Waste* **2013**, *17* (9), 9−15.
(33) Seyedabbasi, M.; Newell, C.; Adamson, D.; Sale, T. Relative contribution of DNAPL and matrix diffusion to the long-term persistence of chlorinated solvent source zones. *J. Contam. Hydrol.* **2012**, *134−135*, 69−81.